Optics Letters

Topologically Enabled Ultrahigh-Q Chiroptical Resonances by Merging Bound States in the Continuum

Shun Wan,[1] Keda Wang,[1] Fatian Wang,[1] Chunying Guan,[1,3] Wenjia Li,[1] Jianlong Liu,[1] Andrey Bogdanov,[2,4] Pavel A. Belov,[2] and Jinhui Shi[1,5]

[1]Key Laboratory of In-Fiber Integrated Optics of Ministry of Education, College of Physics and Optoelectronic Engineering, Harbin Engineering University, Harbin 150001, China
[2]School of Physics and Engineering, ITMO University, 191002 St. Petersburg, Russia
[3]e-mail: cyguan@163.com
[4]e-mail: a.bogdanov@metalab.ifmo.ru
[5]e-mail: shijinhui@hrbeu.edu.cn

Received 27 April 2022; revised 2 June 2022; accepted 7 June 2022; posted 9 June 2022; published 24 June 2022

Ultrahigh-Q chiroptical resonance metasurfaces based on merging bound states in the continuum (BICs) are investigated and numerically demonstrated. The destruction of C_2 symmetry results in the leakage of BICs into quasi-BICs, and a chiral quasi-BIC is obtained by oblique incidence or continuous destruction of the mirror symmetry of the structure. Due to the significant topological properties of merging BICs, the Q factor (over 2×10^5) of the chiral resonance peak obtained is much higher than that of the previous work. Moreover, the proposed structure is easy to fabricate because no additional out-of-plane asymmetry is introduced. The proposed scheme is of importance in chiral biosensing applications.

https://doi.org/10.1364/OL.462021

Growing interest in confining light at the nanoscale has led to a surge in bound states in the continuum (BICs). BICs are embedded eigenmodes of open systems that decoupled from the radiation continuum [1–3]. Being completely confined to space, their radiation Q factor diverges, and resonance width tends to zero. The earliest BIC experimentally observed in optical systems was the symmetry-protected BIC [4], which was prohibited from coupling with the outgoing waves due to symmetry incompatibility. Later, an accidental BIC was discovered [5], in which leakage was canceled by interference. It has been shown that both types of BICs are polarization vortices and have a topological nature. While most topological photonic systems focus on near-field properties, a BIC is a topological phenomenon in non-Hermitian photonic systems associated with leaky states [6–16]. A BIC can exist robustly in reciprocal space as long as the $C_2{}^zT$ and σ_z symmetry of the system is preserved, and its position can be changed by adjusting the structural parameters. In this way, one can combine multiple BICs to produce merging BICs [7–9]. The true BIC is a completely dark state, and it cannot be excited from the far-field. However, breaking the symmetry of the unit cell or incidence under oblique angles results in the appearance of radiative losses [17–21]. BICs turn into quasi-BICs that manifest themselves as Fano or electromagnetically-induced-transparency (EIT) resonance profiles in the electromagnetic spectrum [22,23]. In fact, radiation losses introduced by ineluctable manufacturing imperfections, limited sizes, and material losses cause BICs to radiative losses, which limit the total Q factor and seriously impede the performance of on chip photonic devices. It has been reported that merging BICs have lower radiative losses and are more robust to structure disorder compared to isolated BICs [7–9]. This makes merging BICs an excellent candidate in photonic devices requiring strong light–matter interactions.

Chiral objects cannot be completely superposed with their mirror images by translational and rotational operations [24]. The study of chirality plays an important role in analytical chemistry, crystallography, molecular biology, and the detection of alien life [25]. Chiral structures have different responses to circularly polarized light of different polarization states, namely circular dichroism (CD). For some fields requiring high Q factor, such as chiral sensing, it is an incredible solution to introduce BIC mechanism [26]. Recently, through theoretical derivation and simulation, it has been shown that the chirality of structures can be regulated based on quasi-BICs [27–34]. These works laid the foundation for the investigation of chiral BICs and greatly expanded the technique of optical chirality realization, but nevertheless, most of them require the introduction of out-of-plane asymmetric defects, resulting in increased processing difficulty and cost, otherwise the Q factor of chiral optical response is not high enough.

In this Letter, based on the ideas of merging BICs, ultrahigh-Q chiroptical resonances have been realized by planar metasurfaces in the communication band. By changing the period of the structure, the eight accidental BICs in the same band gradually move to the Γ point, forming the merging BIC and greatly increasing the Q factors of the surrounding modes. The transition from BIC to quasi-BIC is triggered by breaking the in-plane symmetry of the structure. Ultra-chiral quasi-BICs with CD values of 0.93 and 0.97 and Q factors of 2.7×10^5 and 4.8×10^5,

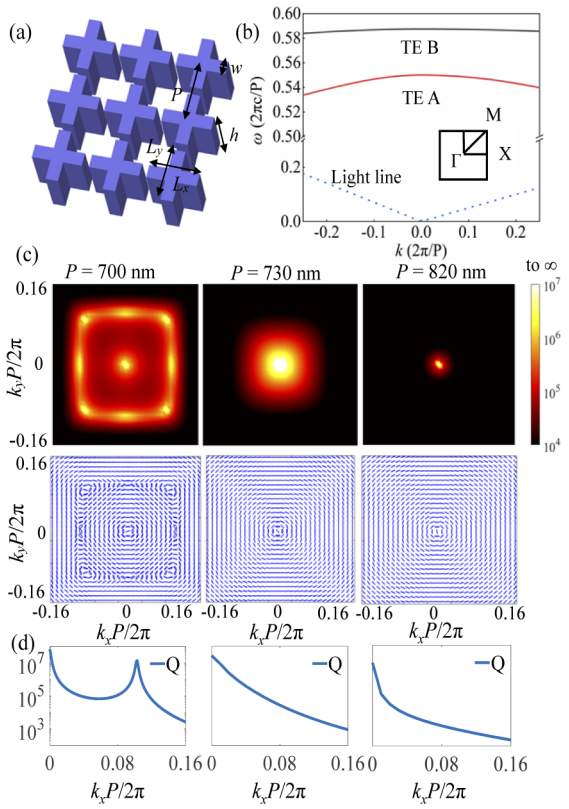

Fig. 1. Formation process and properties of merging BICs. (a) A periodic array of square lattices (infinite) composed of silicon crosses with parameters $L_x = L_y = 640$ nm, $w = 160$ nm, $h = 600$ nm, and $P = 700$ nm. (b) Band structure related to the BIC mode: the red TE A has nine BICs, while TE B has the only one. (c) Above is the Q factor of the TE A band calculated in different periods of the structure and below is the corresponding far-field polarization diagram. The nine BICs carrying topological charges are gradually merged into an isolated BIC with charge +1. (d) The variation of Q factor of modes on the TE A band along the Γ - X direction at different periods.

respectively, are obtained by oblique incidence or further breaking the in-plane mirror symmetry of the structure. Due to the unique topological properties of the merging BIC, the Q factor of chiral quasi-BIC obtained is much higher than that of previous works. We believe that the results obtained have an important role to play in chiral biosensing applications.

The considered metasurface is a periodic array of square lattices (infinite) composed of silicon crosses, as shown in Fig. 1(a), where $L_x = L_y = 640$ nm, $w = 160$ nm, $h = 600$ nm, and $P = 700$ nm. The dispersion of eigenmodes (TE A and TE B) obtained with the finite element method is shown in Fig. 1(b). TE A supports nine BICs, one of which is a symmetry-protected BIC at the Γ point and the others are accidental BICs as the result of destructive interference. However, only one (symmetry-protected) BIC exists on TE B. All of these BICs are the polarization vortices in the far-field. They carry a retained and quantified topological charge that is determined by the number of revolutions of the polarization vector around the BIC, which ensures their robustness. The symmetry-protected BIC will be fixed at the Γ point on account that the C_2 symmetry of the structure is maintained, whereas other BICs move their positions in wave vector space as structural parameters change. Figure 1(c) depicts the changes of Q factors and polarization vector in the BIC merging process. When P =700 nm, nine divergent points can be seen in the plot, representing nine BICs. As the period increases to P =730 nm, the merging BIC appears with a significant increase in the Q factors of the surrounding modes, and the period continues to increase, leaving only a single symmetry-protected BIC. At the bottom of Fig. 1(c) are the polarization vectors around BICs. When $P = 700$ nm, there are nine polarized vortices surrounding BICs. The vortices at the Γ point and the four diagonal vortices rotate counterclockwise around the BIC by 2π, so the topological charge is +1, and the other opposite loops have –1 topological charge [6]. When P =730 nm, all BICs are located at the Γ point, leaving only a +1 charge, and a merging BIC is formed. The three blue lines in Fig. 1(d) represent the variation of Q factors of modes on the TE A band along the Γ - X direction at different periods. It can be seen that the decay rate of the Q factor of the merging BIC is obviously lower than that of the isolated BIC. Three Q curves in Fig. 1(d) are governed by the following rules $Q \propto 1/[k(k + k_{BIC})(k - k_{BIC})]^2$, $Q \propto 1/k^6$ and $Q \propto 1/k^2$ [7]. It has been proved that the unique topological characteristics of the merging BIC can reduce the radiation loss caused by the limited sample size, manufacturing defects, and other factors, thus further improving the Q factor of the resonator [7].

After determining the structural parameters that can generate the merging BIC, we begin to investigate how to make the system produce a chiral response. Considering a time-dependent wave $e^{-i\omega t}$ propagating in the negative direction z, circular dichroism (CD) is defined by the following formula [31]:

$$CD_T = \frac{|t_R|^2 - |t_L|^2}{|t_R|^2 + |t_L|^2}, CD_R = \frac{|r_R|^2 - |r_L|^2}{|r_R|^2 + |r_L|^2} \quad (1)$$

where $|t_R|^2$ represents the transmittance of right circularly polarized (RCP) light, $|t_L|^2$ is the transmittance of left circularly polarized (LCP) light, $|r_R|^2$ is the reflectance of RCP, and $|r_L|^2$ is the reflectance of LCP. Typically, this problem is usually described by S-matrix equation that combines the output wave amplitudes $b_\pm$ and $b'_\pm$, with the input wave amplitudes $a_\pm$ and $a'_\pm$, where $b_\pm$ and $b'_\pm$, $a_\pm$ and $a'_\pm$ represent the entry and exit from different sides, respectively [32]:

$$\begin{pmatrix} b_+ \\ b'_+ \\ b_- \\ b'_- \end{pmatrix} = \begin{pmatrix} r & t_L & 0 & 0 \\ t_R & r' & 0 & 0 \\ 0 & 0 & r & t_R \\ 0 & 0 & t_L & r' \end{pmatrix} \begin{pmatrix} a_+ \\ a'_+ \\ a_- \\ a'_- \end{pmatrix} \quad (2)$$

According to CMT theory, the origin of chirality can be explained [27]:

$$t_R = \tau - \frac{m_+ m'_-}{i(\omega - \omega_0) - \gamma_0}, t_L = \tau - \frac{m'_+ m_-}{i(\omega - \omega_0) - \gamma_0} \quad (3)$$

where τ is the magnitude of the background transmission, the resonant frequency ω_0 and the damping γ_0 are independent of the helix, $m_\pm$ are the eigenstate coupling parameters of the incident wave corresponding to the helicity on one side of the metasurface, and $m'_\pm$ are the eigenstate coupling parameters on the other side of the metasurface. It can be concluded from the above equation that optical chirality is determined by the degree of chirality coupling between the eigenstate and free space. Damping γ_0 is the sum of all losses, equal to the radiation loss (γ_r) plus the dissipative loss (γ_d): $\gamma_0 = \gamma_r + \gamma_d$, where γ_r is determined by

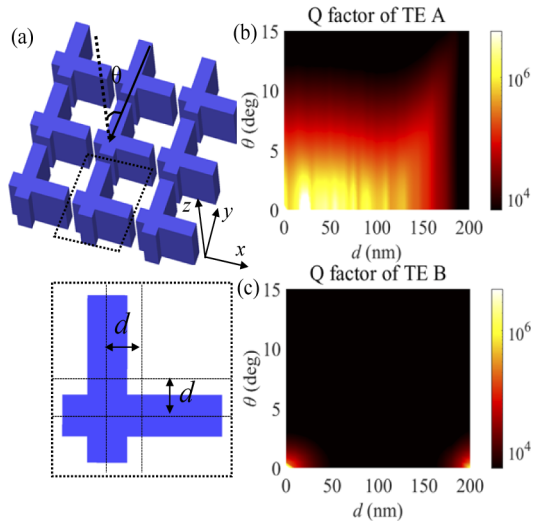

Fig. 2. Relation between Q factor of quasi-BIC and the in-plane asymmetry factor d and incidence angle θ. (a) Structure diagram. (b) The Q factor of the merging BIC on TE A when $P = 730$ nm varies with d and θ. (c) The Q factor of the isolated BIC on TE B when P = 730 nm varies with d and θ.

the coupling [29]:

$$2\gamma_r = |m_+|^2 + |m'_+|^2 = |m_-|^2 + |m'_-|^2 \tag{4}$$

The transmission difference is expressed as [27]

$$|t_R|^2 - |t_L|^2 = 2\gamma_d \frac{|m_-|^2 - |m_+|^2}{(\omega - \omega_0)^2 + (\gamma_r + \gamma_d)^2} \tag{5}$$

Therefore, to obtain optical chirality, it is necessary to accurately control the coupling between the eigenstate and the free-space continuum, and the structure has different response degrees to incident waves with different circularly polarized waves.

In the first step, the C_2 symmetry of the structure is broken by moving the horizontal silicon strip and the vertical silicon strip down and to the left by a distance d, respectively, to excite the quasi-BIC, as illustrated in Fig. 2(a). Then, we empower the system external chirality by tilting the incident angle (θ) to break the out-of-plane mirror symmetry of the structure [25,31]. The incidence angle θ is the angle between the incidence beam and the z axis. In fact, the addition of a substrate will also destroy the out-of-plane symmetry of the structure, resulting in an unexpected chirality response under the normal incidence. In order to eliminate this effect, the structure can be practically wrapped in a homogeneous isotropic medium. It is known to us that both the tilted incident angle and the disturbance breaking C_2 symmetry can transform a BIC into a quasi-BIC, so we first calculate the relationship between resonances Q factor and these two parameters, as shown in Figs. 2(b) and 2(c), where the merging BIC on TE A and the isolated BIC on TE B are presented, respectively. By comparing Figs. 2(b) and 2(c), it is clear that the Q factor of the merging BIC is several orders of magnitude higher than that of the isolated BIC for the same structural parameters. For the case of high Q in the lower right corner of Fig. 2(c), the accidental BIC is generated due to interference cancellation.

Figure 3(a) shows the spectra of CD_R for different incident angles when d =140 nm. As the angle increases, the CD_R first

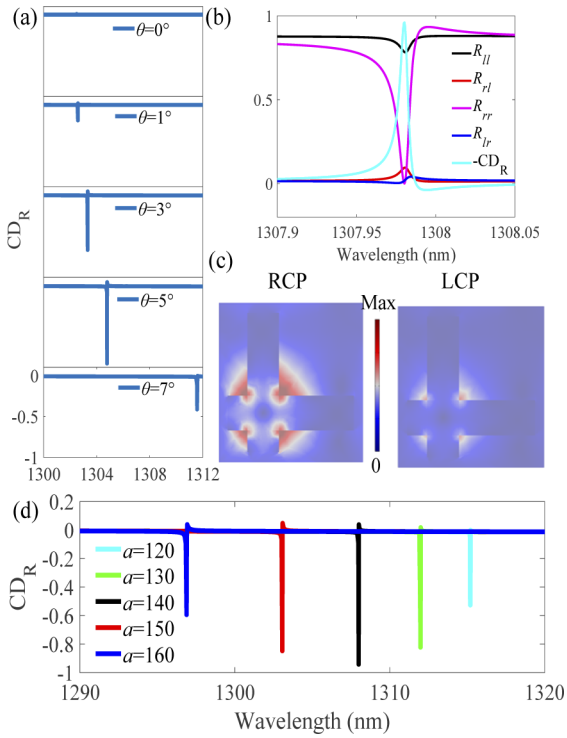

Fig. 3. Chirality response characteristics of the quasi-BIC at oblique incidence. (a) The variation of magnitudes CD of circular dichroism for reflected waves with incident angle when d =140 nm. (b) shows the reflectance spectra (R_{lr}, R_{rl}, R_{rr}, R_{ll}) and $-CD_R$ of the structure when $d = 140$ nm, and $\theta = 5°$. (c) The electromagnetic field distribution of the quasi-BIC when RCP (left) and LCP (right) incident. (d) The variation of magnitudes CD of circular dichroism for reflected waves with the structural parameters when $\theta = 5°$.

increases and then decreases, and it reaches its maximum value at $\theta = 5°$. Figure 3(b) shows the reflectance and CD spectra: $R_{lr} = |r_{lr}|^2$, $R_{rl} = |r_{rl}|^2$, $R_{rr} = |r_{rr}|^2$, $R_{ll} = |r_{ll}|^2$, and $-CD_R$ of the structure; at this point, the system has a CD_R of about 0.93 and a Q factor of about a staggering 273,300. It can be seen from Fig. 3(b) that the structure reflects different intensities of LCP and RCP, that is to say, the coupling intensities of the two kinds of light are different. The different responses can also be confirmed by the electric field in Fig. 3(c). The coupling strength of the system to RCP is much greater than that to LCP. From the above results, it can be concluded that quasi-BICs can exhibit high Q and strong chiroptical response by appropriately selecting structural parameters and incident angles. Moreover, thanks to the unique topological properties of the merging BIC, the Q factor is much larger than that of the previous work in Refs. [30,31,34].

Because the structure still retains partial symmetry, an oblique incident angle is required to give external chirality. Next, by breaking both in-plane inversion and mirror symmetry of the dielectric metasurface, high Q chiroptical resonance can be achieved under normal incidence. As shown in Fig. 4(a), the symmetry of the structure is further broken by shortening the vertical silicon strip in Fig. 3(a) to give the structure intrinsic chirality. Figure 4(b) shows the reflectance spectra (R_{lr}, R_{rl}, R_{rr}, R_{ll}) and CD_R of the structure when $b = 160$ nm and $d = 30$ nm. After calculation, the maximum amplitude of CD is about 0.97, and the Q factor exceeds 480,000, which is significantly higher

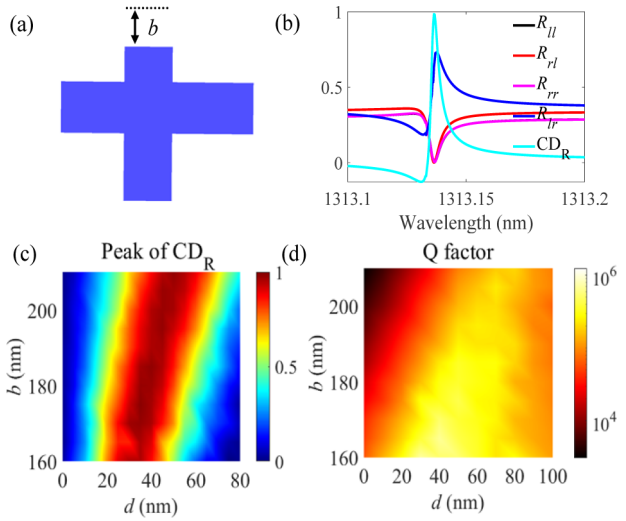

Fig. 4. Chirality response characteristics of quasi-BIC at normal incidence. (a) Schematic diagram of structural element. (b) The Jones matrix and CD_R of the structure at $d = 30$ nm and $b = 160$ nm. (c) Maximum CD_R value of the system under different structural parameters. (d) Q factor of the system under different structural parameters.

than previous studies. Figures 4(c) and 4(d), respectively, show the maximum CD_R value and Q factor of the system under different structural parameters. It can be seen that the structure maintains high Q factor and CD_R over a wide range.

In summary, by designing structures that support the merging BIC and progressively break its symmetry, we obtain strong chiroptical resonances with ultrahigh-Q factor. Since there is no out-of-plane asymmetry factor introduced, the structure is relatively easy to manufacture. In addition, due to the unique topological properties of the merging BIC, the Q factor of the chiroptical resonances is much larger than that of the previous work. The results can be applied to chiral biosensors with high spectral resolution, nonlinear chiroptics with high efficiency, low-threshold circular polarized lasing, and security applications.

Funding. National Natural Science Foundation of China (62175049); Natural Science Foundation of Heilongjiang Province (ZD2020F002); 111 project (B13015); Fundamental Research Funds for the Central Universities (3072021CF2508, 3072021CFT2501); Russian Science Foundation (21-72-30018); Basis Foundation.

Disclosures. The authors declare no conflicts of interest.

Data availability. Data underlying the results presented in this paper are not publicly available at this time but may be obtained from the authors upon reasonable request.

REFERENCES

1. J. von Neumann and E. Wigner, Phys. Z. **30**, 465 (1929).
2. H. Friedrich and D. Wintgen, Phys. Rev. A **32**, 3231 (1985).
3. C. W. Hsu, B. Zhen, A. D. Stone, J. D. Joannopoulos, and M. Soljačić, Nat. Rev. Mater. **1**, 16048 (2016).
4. Y. Plotnik, O. Peleg, F. Dreisow, M. Heinrich, S. Nolte, A. Szameit, and M. Segev, Phys. Rev. Lett. **107**, 183901 (2011).
5. C. W. Hsu, B. Zhen, J. Lee, S.-L. Chua, S. G. Johnson, J. D. Joannopoulos, and M. Soljačić, Nature **499**, 188 (2013).
6. B. Zhen, C. W. Hsu, L. Lu, A. D. Stone, and M. Soljačić, Phys. Rev. Lett. **113**, 257401 (2014).
7. J. Jin, X. Yin, L. Ni, M. Soljačić, B. Zhen, and C. Peng, Nature **574**, 501 (2019).
8. M. Kang, S. Zhang, M. Xiao, and H. Xu, Phys. Rev. Lett. **126**, 117402 (2021).
9. M.-S. Hwang, H.-C. Lee, K.-H. Kim, K.-Y. Jeong, S.-H. Kwon, K. Koshelev, and Y. Kivshar, Nat. Commun. **12**, 14135 (2021).
10. H. M. Doeleman, F. Monticone, W. den Hollander, A. Al, and A. F. Koenderink, Nat. Photonics **12**, 397 (2018).
11. Y. Zhang, A. Chen, W. Liu, C. W. Hsu, B. Wang, F. Guan, X. Liu, L. Shi, L. Lu, and J. Zi, Phys. Rev. Lett. **120**, 186103 (2018).
12. B. Wang, W. Liu, M. Zhao, J. Wang, Y. Zhang, A. Chen, F. Guan, X. Liu, L. Shi, and J. Zi, Nat. Photonics **14**, 623 (2020).
13. W. Ye, Y. Gao, and J. Liu, Phys. Rev. Lett. **124**, 153904 (2020).
14. B. Yan, Y. C. Peng, A. Q. Shi, J. L. Xie, P. Peng, and J. J. Liu, Opt. Express **47**, 2044 (2022).
15. Y. Wei, B. Yan, Y. Peng, A. Shi, D. Zhao, R. Peng, Y. Xiang, and J. Liu, Opt. Express **46**, 3941 (2021).
16. A. Q. Shi, B. Yan, R. Ge, J. L. Xie, Y. C. Peng, H. Li, W. E. I. Sha, and J. J. Liu, Opt. Express **46**, 1089 (2021).
17. K. Koshelev, Y. Tang, K. Li, D.-Y. Choi, G. Li, and Y. Kivshar, ACS Photonics **6**, 1639 (2019).
18. Y. Wang, Z. Han, Y. Du, and J. Qin, Nanophotonics **10**, 1295 (2021).
19. K. Koshelev, S. Lepeshov, M. Liu, A. Bogdanov, and Y. Kivshar, Phys. Rev. Lett. **121**, 193903 (2018).
20. L. Carletti, K. Koshelev, C. De Angelis, and Y. Kivshar, Phys. Rev. Lett. **121**, 033903 (2018).
21. H. S. Nguyen, F. Dubois, T. Deschamps, S. Cueff, A. Pardon, J. L. Leclercq, C. Seassal, X. Letartre, and P. Viktorovitch, Phys. Rev. Lett. **120**, 066102 (2018).
22. Z. Liu, Y. Xu, Y. Lin, J. Xiang, T. Feng, Q. Cao, J. Li, S. Lan, and J. Liu, Phys. Rev. Lett. **123**, 253901 (2019).
23. M. F. Limonov, M. V. Rybin, A. N. Poddubny, and Y. S. Kivshar, Nat. Photonics **11**, 543 (2017).
24. Y. Chen, J. Gao, and X. Yang, Nano Lett. **18**, 520 (2018).
25. J.J. Wu, X. T. Xu, X. Q. Su, S. Zhao, C. Wu, Y. Sun, Y. H. Li, F. Wu, Z. W. Guo, H. T. Jiang, and H. Chen, Phys. Rev. Appl. **16**, 064018 (2021).
26. Y. Chen, C. Zhao, Y. Z. Zhang, and C. W. Qiu, Nano Lett. **20**, 8696 (2020).
27. M. V. Gorkunov, A. A. Antonov, and Y. S. Kivshar, Phys. Rev. Lett. **125**, 093903 (2020).
28. A. Overvig, N. Yu, and A. Alu, Phys. Rev. Lett. **126**, 073001 (2021).
29. M. V. Gorkunov, A. A. Antonov, V. R. Tuz, A. S. Kupriianov, and Y. S. Kivshar, Adv. Opt. Mater. **9**, 2100797 (2021).
30. K. Kim and J. Kim, Adv. Opt. Mater. **9**, 2101162 (2021).
31. T. Shi, Z.-L. Deng, G. Geng, Y. Zeng, G. Hu, A. Overvig, J. Li, C.-W. Qiu, A. Alù, Y. S. Kivshar, and X. Li, "Planar chiral metasurfaces with maximal tunable chiroptical response driven by bound states in the continuum," arXiv:2112.07122 (2021).
32. A. V. Kondratov, M. V. Gorkunov, A. N. Darinskii, R. V. Gainutdinov, O. Y. Rogov, A. A. Ezhov, and V. V. Artemov, Phys. Rev. B **93**, 195418 (2016).
33. M. Gandolfi, A. Tognazzi, D. Rocco, C. De Angelis, and L. Carletti, Phys. Rev. A **104**, 023524 (2021).
34. J. G. Hu, Y. X. Xiao, L.-M. Zhou, X. Y. Jiang, W. Qiu, W. Feu, Y. Chen, and Q. W. Zhan, Opt. Express **30**, 16020 (2022).